ME 155C Final Report: System Identification and Optimal Control of an Inverted Pendulum on a Cart

Vedad Bassari, Steven Man

June 25, 2023

1 Abstract

For our final project, we performed system identification and optimal control of an inverted pendulum on a cart. We plan to control the angular position of the encoder for the pendulum mass. We can measure the cart encoder, the pendulum mass encoder, and the input voltage for the cart's motor. We targeted and achieved the following closed-loop performance metrics: 5° tracking error in angular position, 60° phase margin, disturbance rejection with respect to manually introduced disturbances, noise attenuation above the sampling frequency, and stability.

2 Introduction

The objective of this project is to design a controller to regulate the angular position of an inverted-pendulum cart system. The system consists of a motor-driven cart attached to a pendulum mass via a free rotational joint. The angular position of the pendulum is measured by an incremental encoder, which provides the state that we wish to control. To achieve this goal, the voltage input to the motor must be chosen according to a control law that fulfills the desired performance metrics as follows:

- Stabilize the closed-loop system.
- 60° phase margin
- 5° tracking error in angular position
- Achieve the minimum settling time possible.
- Limit control input to hardware's constraints.
- 95% noise attenuation at high frequencies
- 95% disturbance attenuation at low frequencies

In the following sections, we performed parametric identification and modeling of the system, thus determining the transfer function relating the input voltage to the cart position and the pendulum position, as well as the state-space model. We then designed an LQR controller and implemented LQG for linear state estimation. The resulting closed-loop system characteristics are presented in both simulation and experiments.

3 System Identification

The objective of system identification is to find the governing relationships that determine the system's output (cart position [encoder count] and pendulum angular position [encoder count]) based on the system's inputs (motor voltage [V]). We present two approaches to system identification: an analytical formulation of the state-space model for the system, and an experimental characterization of the system's complex-domain transfer functions.

3.1 State-space Modeling

The following schematic describes the dynamics of the system that we are trying to control. p is the displacement of the cart along the track and θ is the pendulum's angular position from vertical.

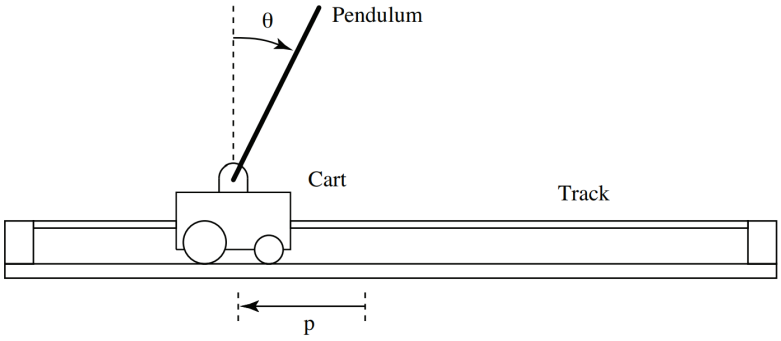

Figure 1: Inverted pendulum cart schematic

By breaking the system down into its components, we obtain the following free-body diagram. R is the reaction force of the ground on the car. N and P are the reaction forces between the pendulum and the cart. g is the gravitational acceleration. m_c and m_p are the mass of the cart and the pendulum respectively. F is the force applied to the cart.

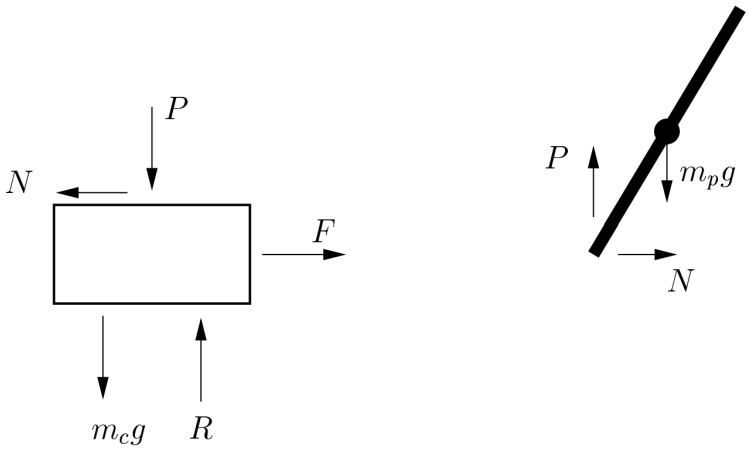

Figure 2: Inverted pendulum cart free body diagram

Applying Newton's second law in both the horizontal and vertical directions, we obtain the following

equations of motion:

$$F = (m_c + m_p)\ddot{p} + m_p l\cos(\theta)\ddot{\theta} - m_p l\sin(\theta)(\dot{\theta})^2 \tag{1}$$

$$\ddot{\theta}(I + m_p l^2) = m_p g l\sin(\theta) - m_p l\ddot{p}\cos(\theta) \tag{2}$$

Using the motor's voltage-force relationship, we rewrite the force F in terms of voltage V, velocity, and cart parameters:

$$F = \frac{K_m K_g}{Rr}V - \frac{K_m^2 K_g^2}{Rr^2}\dot{p} \tag{3}$$

We can then plug in the force equation as well as linearize the equations of motion about $\theta = 0$:

$$\ddot{p}\left(M - \frac{m_p l}{L}\right) = \frac{K_m K_g}{Rr}V - \frac{K_m^2 K_g^2}{Rr^2}\dot{p} - \frac{m_p l g}{L}\theta \tag{4}$$

$$\ddot{\theta}\left(L - \frac{m_p l}{M}\right) = g\theta - \frac{1}{M}\left(\frac{K_m K_g}{Rr}V - \frac{K_m^2 K_g^2}{Rr^2}\dot{p}\right) \tag{5}$$

Where:

$$M = m_c + m_p$$
$$L = \frac{I + m_p l^2}{m_p l}$$

Using the following state-vector:

$$\vec{x} = \begin{bmatrix} x_1 \\ x_2 \\ x_3 \\ x_4 \end{bmatrix} = \begin{bmatrix} p \\ \dot{p} \\ \theta \\ \dot{\theta} \end{bmatrix}$$

We obtain the state-space matrices:

$$\dot{\vec{x}} = A\vec{x} + Bu \tag{6}$$
$$\vec{y} = C\vec{x} \tag{7}$$

where $u = V$, and (with parameters listed in table 1):

$$A = \begin{bmatrix} 0 & 1 & 0 & 0 \\ 0 & \frac{K_m^2 K_g^2}{Rr^2\left(\frac{m_p l}{L} - M\right)} & \frac{g m_p l}{L\left(\frac{m_p l}{L} - M\right)} & 0 \\ 0 & 0 & 0 & 1 \\ 0 & \frac{K_m^2 K_g^2}{Rr^2 M\left(L - \frac{m_p l}{M}\right)} & \frac{g}{L - \frac{m_p l}{M}} & 0 \end{bmatrix} = \begin{bmatrix} 0 & 1 & 0 & 0 \\ 0 & -15.44 & -3.16 & 0 \\ 0 & 0 & 0 & 1 \\ 0 & 37.97 & 31.89 & 0 \end{bmatrix}$$

$$B = \begin{bmatrix} 0 \\ \frac{K_m K_g}{Rr\left(M - \frac{m_p l}{L}\right)} \\ 0 \\ \frac{K_m K_g}{RrM\left(L + \frac{m_p l}{M}\right)} \end{bmatrix} = \begin{bmatrix} 0 \\ 3.46 \\ 0 \\ -8.50 \end{bmatrix}; \qquad C = \begin{bmatrix} 1 & 0 & 0 & 0 \\ 0 & 0 & 1 & 0 \end{bmatrix}$$

Parameters			
K_m	0.00767 $\frac{Nm}{A}$	m_c	0.451 kg
K_g	3.7 (Gear-box ratio)	m_p	0.217 kg
R	2.56 Ω	l	0.305 m
r	0.00635 m	I	0.0067 $kg \cdot m^2$

Table 1: Pendulum cart system parameters

3.2 Parametric Identification

We performed parametric identification on the downward pendulum system to obtain the transfer functions from voltage to pendulum position and motor cart position.

Parametric system identification attempts to numerically resolve the transfer function that describes a linear process by linear regression. A time-domain transfer function of the form:

$$\beta(\frac{d}{dt})y_f - \alpha(\frac{d}{dt})u_f \tag{8}$$

with u_f and y_f as the filtered inputs and outputs respectively are cast as a CARX model:

$$\frac{d^n y}{dt^n} = \phi \cdot \theta \tag{9}$$

for which the mean squared error, $MSE = \frac{1}{N}||Y - \phi\hat{\theta}||$, is minimized over the parameter vector $\hat{\theta}$. Note that in this formulation, ϕ is a matrix constructed from the derivatives of the system inputs and outputs which are calculated directly in the complex domain.

In this formulation, the quality of the regression is represented by the normalized error and the identifiability of the system (an indicator of non-singularity of the matrices) which is inferred from the covariance matrix. Several factors contribute to the quality of regression, including A) Frequency-content richness and magnitude of the input signals, B) Accuracy of model order estimation (i.e. the assumed form of the transfer function), and C) Numerical stability of the input/output data, often addressed by normalization to the interval [-1,1]. To ensure the richness of the input signals, a mix of four chirp and square-wave signals were used over a range of frequencies similar to the non-parametric identification experiments. Additionally, the same value of input magnitude $\alpha = 0.75$ was employed.

As detailed above, model order estimation is the other major contributor to the quality of parametric identification. In this project, parametric identification was performed on the experimental data using the **tfest()** function for various values of poles and zeros to identify the appropriate model order. In specific, three guidelines were used to identify the appropriate model order:

- The normalized MSE was plotted for different model orders; order estimates that yielded a high MSE were eliminated due to a lack of sufficient poles and zeros.
- The largest standard deviation of the diagonal elements of the covariance matrix was plotted to indicate identifiability; estimates resulting in a high standard deviation were eliminated due to over-fitting.
- The root-locus plots of the different estimate transfer functions were generated and estimations that yielded pole-zero cancellations or comparatively large poles were eliminated as indicators of over-fitting.

Figure 3 shows the MSE and standard deviation plots for various pole-zero identifications along with the corresponding Bode plots (3 poles 2 zeros for the cart, and 3 poles 0 zeros for the pendulum). The selection was guided by the three criterea mentioned above.

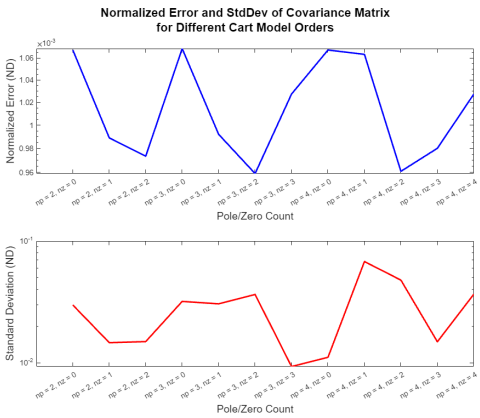

(a) Normalized error and standard deviation of linear regression for different number of poles and zeros

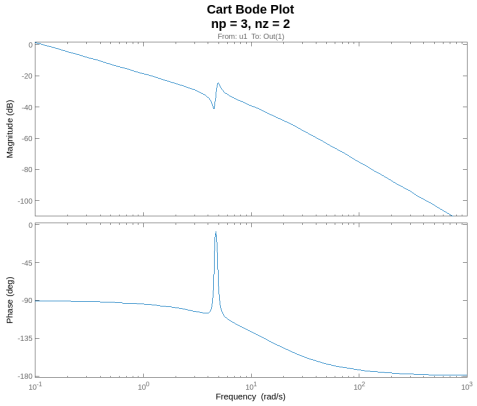

(b) Bode plots of best model-order candidates

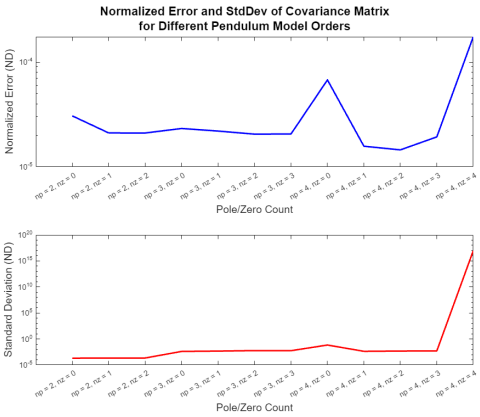

(c) Normalized error and standard deviation of linear regression for different number of poles and zeros

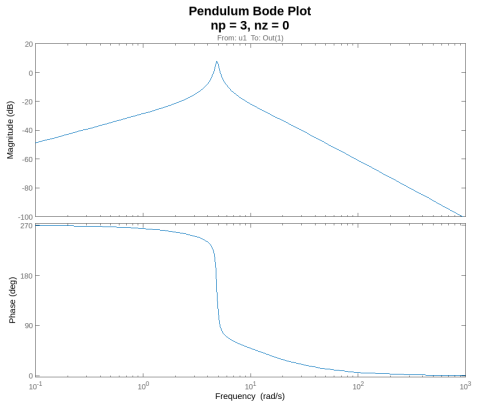

(d) Bode plots of best model-order candidates

Figure 3: Results from parametric identification with different enforced numbers of poles and zeros

3.3 Model Validation

To implement LQR control, we need a state-space representation of the pendulum-cart system. To show that the transfer functions we obtained through parametric identification are very similar to the state-space modeling with physical parameters, we compared the root locus plots of the same system modeled from the two methods mentioned above in Figure 4.

This validation allowed us to proceed to design an LQR controller to control the pendulum position using the state-space model we derived.

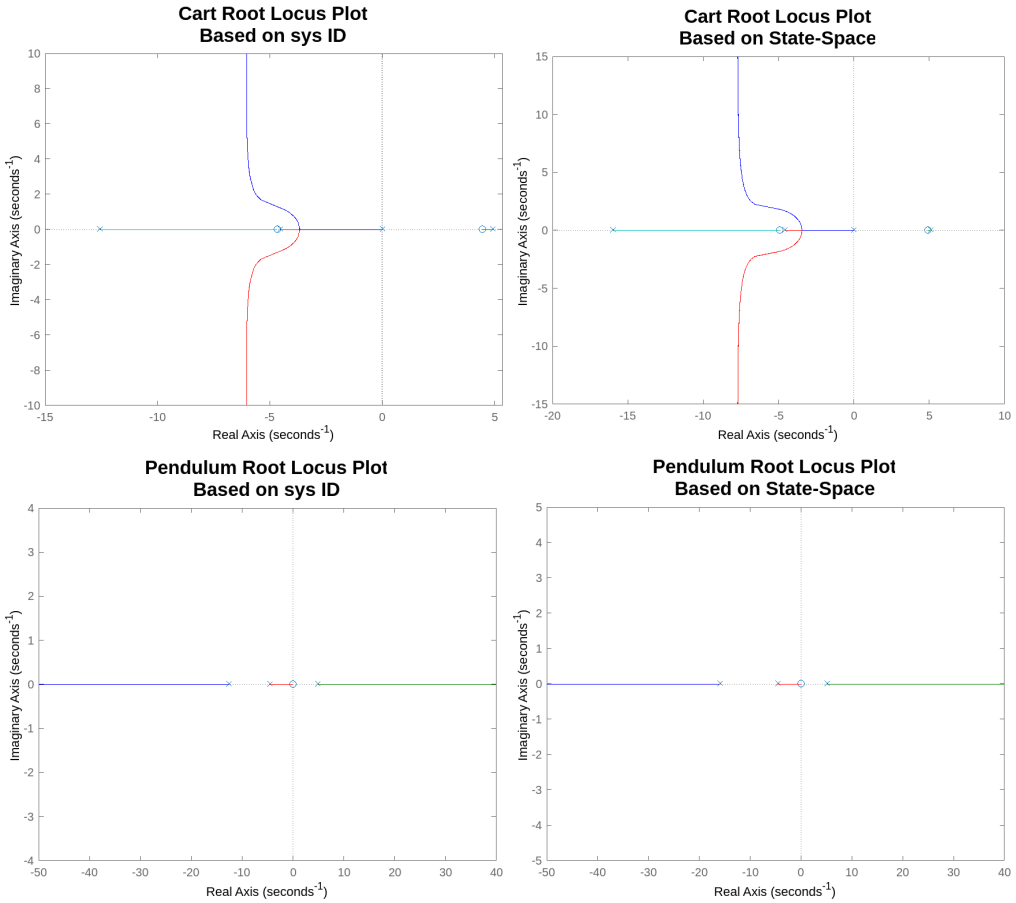

Figure 4: Root locus of transfer functions obtained from system identification compared to root locus of the state-space system derived from modeling.

4 Controller Design

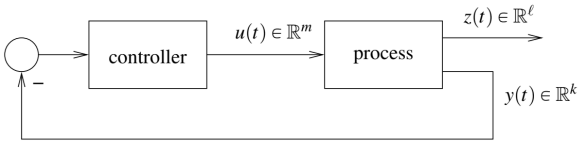

Figure 5: Block diagram with LQR controller.

Using the state-space model presented in section 3.1, we designed an optimal proportional control law that minimizes the cost function

$$J_{LQR} = \int_0^{\inf} ||z(t)||^2 + \rho||u(t)||^2 dt \tag{10}$$

which corresponds to the block diagram shown in Figure 6. In this setting, the controller is a proportional matrix K acting on the measured y(t). This is a formulation known as the Linear-Quadratic Regulator (LQR). We note that this formulation takes the state z to 0. Moreover, we observe that we are free in our choice of

z and ρ to obtain the desired system specifications. In order to guide our controller design, we first define open-loop specifications that correspond to the desired closed-loop characteristics outlined in section 2.

Closed-Loop Characteristics	**Open-Loop Specifications**
Stability, 60 degree phase margin	Nyquist Criterion
5% Tracking Error at $\omega = 0\ \frac{rad}{s}$	21 dB
95% Disturbance Rejection at $\omega = 0\ \frac{rad}{s}$	54 dB
95% Disturbance Rejection at $\omega = 1000\ \frac{rad}{s}$	0.05 dB
Safe Maximum Input	5 V

Table 2: Closed-loop performance of the regulated system, n = 5.

4.1 Control System Modeling

Firstly, the output vector was chosen as $z = [x, \theta]^T$ to fulfill the Nyquist criterion by rendering z independent of the input u in accordance with [1] (H = 0). This property guarantees the LQR control is stable and has a 60-degree phase margin, in addition to providing robustness with respect to small multiplicative uncertainty. Next, the value of ρ was modulated to fulfill the remaining open-loop gain requirements, with the results shown in Figure 5. The MATLAB function **LQR(A,B,QQ,RR)** was used to solve the algebraic Ricatti equation that estimates the controller K. Subsequently, $\rho = 0.005$ was chosen as the least energy-intensive choice that fulfilled the design requirements. We note that the LQR controller yields strong low-frequency performance, but we do not have control over the high-frequency behavior of the system, limiting noise attenuation.

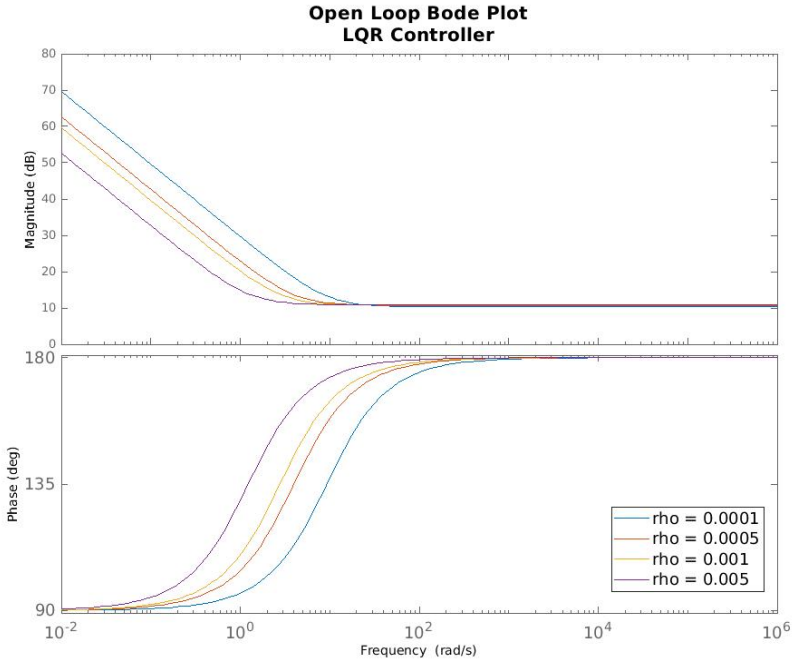

Figure 6: Open-loop Bode plots of the system under LQR action for various values of ρ.

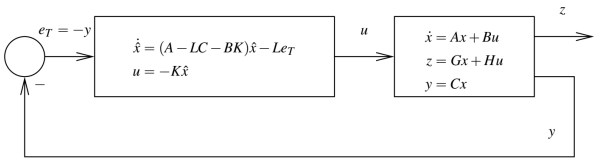

Figure 7: Block diagram with LQR/LQG controller.

There is a major practical limitation in the implementation of the controller designed above; namely, this regulator requires the full state of the system to be provided to the proportional action. However, the encoders available in the system only monitor position and angle, rather than linear and angular velocity. This limitation means that velocities are obtained through finite differencing, which results in noisy measurements. This limitation can be addressed by monitoring the system using a linear state estimator (LQG) that corrects itself using position measurements. This procedure, represented in block diagrams by Figure 7, is outlined in many control systems textbooks, including [2]. This estimator was implemented in MATLAB using the function **kalman(sys,QN,RN)**. Finally, the state-space model of the full controller was obtained from **reg(sys,K,L)** using the proportional gain K and the linear estimator L.

The implementation of the LQG/LQR controller improves the open-loop characteristics of the LQR system in the higher frequency regimes. However, we wish to maintain the low-frequency behavior - this is done according to the loop-gain recovery principle by setting σ - a parameter of the Gaussian distribution used in the LQG formulation - to be sufficiently small. σ dictates how conservative the estimator's corrective term is, with smaller values of sigma resulting in sharper adjustments to the state estimation. Figure 8 highlights the parametric variation of the open-loop Bode plots with respect to σ. We chose $\sigma = 10e - 8$ to have loop gain recover up to nearly 100 $\frac{rad}{s}$. The annotations highlight the design's capability in low-frequency tracking error and disturbance rejection as well as high-frequency noise attenuation according to table 2.

4.2 Closed-loop Characteristics

The controller design in the previous section was implemented in hardware and the closed-loop characteristics of the system were examined. Figure 10 shows the bode plots of closed-loop transfer functions for both the pendulum and the cart. We observe the effectiveness of the regulator over the frequency regime of interest, namely 0-100 $\frac{rad}{s}$.

The system was then manually perturbed, and the system response was compared to the theoretical prediction as shown in Figure 9. The hardware system generally follows the same trends as predicted numerically, but demonstrates substantially longer transients and larger steady-state errors. This is most likely due to

- Errors in the state-space model formulation
- Error in the initiation of the system in the perfectly upright position
- Sensor noise.

Finally, table 3 highlights several relevant closed-loop characteristics obtained from the hardware setup. We observe that despite the favorable phase margin provided by the controller, the large inertia of the pendulum results in an appreciable overshoot. However, the remaining characteristics indicate desirable performance with respect to the design benchmarks.

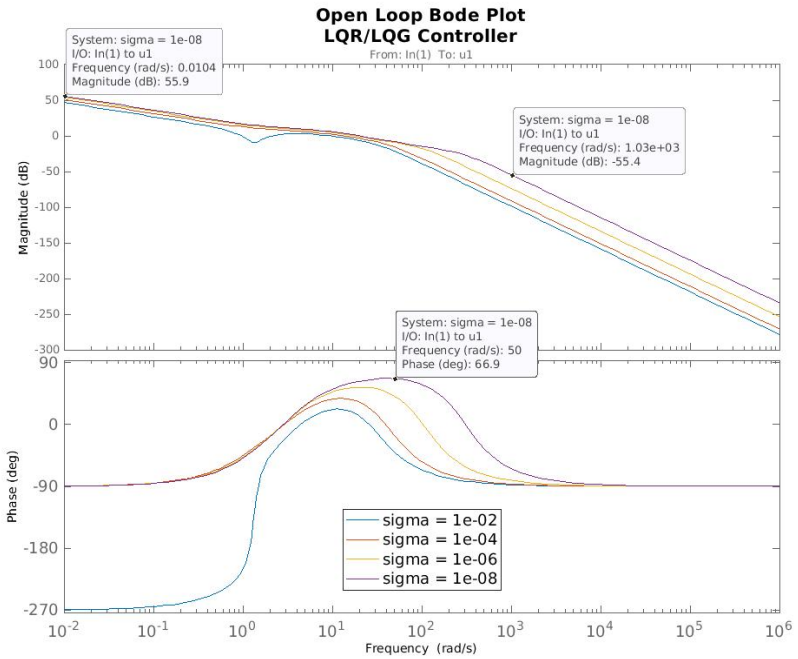

Figure 8: Open-loop Bode plots of the system under LQR/LQG action for various values of σ.

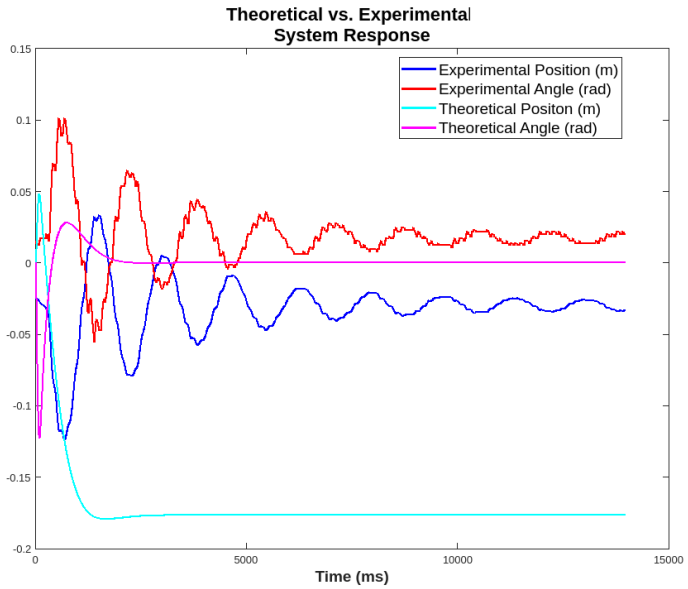

Figure 9: Theoretical system response to arbitrary initial conditions overlayed with experimental response.

	Mean	**Standard Deviation**
Settling Time (s)	5.65	0.7
Maximum Overshoot (%)	33.1	5
Steady-state Error (rad)	0.0153	0.008
Maximum Disturbance (rad)	0.101	0.07
Maximum Input (V)	4.06	0.5

Table 3: Closed-loop performance of the regulated system, n = 3.

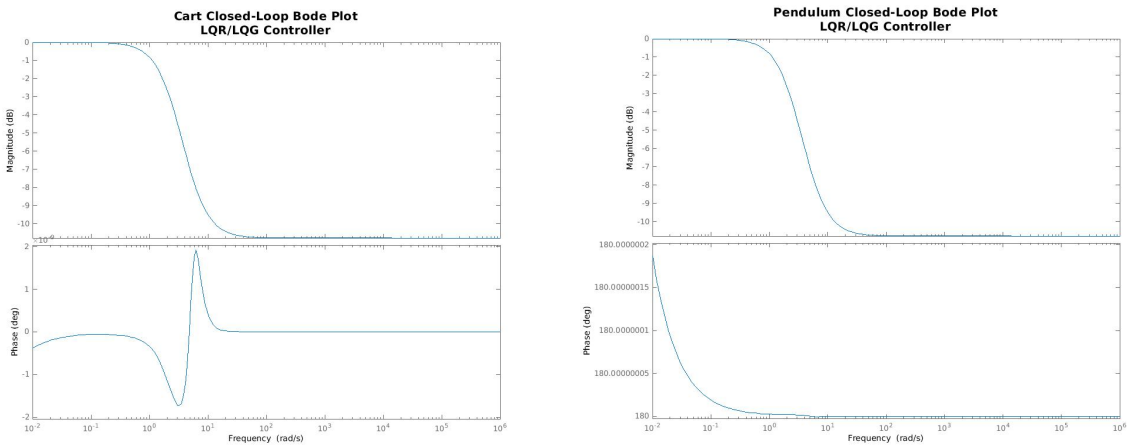

(a) Cart

(b) Pendulum

Figure 10: Closed-loop Bode plots of the cart and the pendulum indicating strong low-frequency regulation.

4.3 Conclusions and Future Work

In this discussion, we covered the full process of characterizing and controlling an inverted pendulum on a linear cart. We first identified the system parametrically and analytically using experimental data and mechanical modeling. Next, we used our identification results to recommend an optimal control law based on a set of application-specific performance constraints. Finally, we implemented, modified, and characterized the proposed LQR controller to confirm its performance. Several additional considerations were not emphasized in our controller design: importantly, we did not quantitatively analyze the robustness of the controller to identification errors. Additionally, we avoided operating in the non-linear regime of the system to simplify the control problem. Each of these modifications could be implemented to develop a more capable control system.

References

[1] J. Hespanha, *Advanced Undergraduate Topics in Control Systems Design*, 2023. [Online]. Available: https://web.ece.ucsb.edu/ hespanha/published/allugtopics-20230402.pdf

[2] K. Ogata, *Modern Control Engineering*, ser. Instrumentation and controls series. Prentice Hall, 2010. [Online]. Available: https://books.google.com/books?id=Wu5GpNAelzkC